

VLSS Redux: Software Improvements applied to the Very Large Array Low-frequency Sky Survey

W. M. Lane,¹ W. D. Cotton,² J. F. Helmboldt,¹ N. E. Kassim,¹

We present details of improvements to data processing and analysis which were recently used for a re-reduction of the Very Large Array (VLA) Low-frequency Sky Survey (VLSS) data. Algorithms described are implemented in the data-reduction package Obit, and include smart-windowing to reduce clean bias, improved automatic radio frequency interference removal, improved bright-source peeling, and higher-order Zernike fits to model the ionospheric phase contributions. An additional, but less technical improvement was using the original VLSS catalog as a same-frequency/same-resolution reference for calculating ionospheric corrections, allowing more accuracy and a higher percentage of data for which solutions are found. We also discuss new algorithms for extracting a source catalog and analyzing ionospheric fluctuations present in the data. The improved reduction techniques led to substantial improvements including images of six previously unpublished fields (1% of the survey area) and reducing the clean bias by 50%. The largest angular size imaged has been roughly doubled, and the number of cataloged sources is increased by 35% to 95,000.

1. Introduction

The Very Large Array (VLA) Low-frequency Sky Survey (VLSS), released in *Cohen et al.* [2007] covers 95% of the 3π sr of sky area above -30° declination at a frequency of 74 MHz, a resolution of approximately $80''$, and an RMS sensitivity of ≈ 0.1 Jy/bm. The main survey products consist of a publicly available catalog and a set of maps. The survey was intended to serve as a low-frequency counterpart to the National Radio Astronomy Observatory (NRAO)-VLA Sky Survey (NVSS) at 1400 MHz [*Condon et al.*, 1998], allowing spectral information to be compiled for statistical samples of sources. It also provides a low-frequency sky model.

The original data reduction was hampered by limited software. In the past few years, several major improvements to the processing software along with the availability of faster computers which could process the data in a fraction of the time originally needed, made it attractive to re-reduce the survey

data. The goal of the re-reduction was to increase the sensitivity and uniformity of the survey and maps. The pipeline data processing developed could also be leveraged as a basis for future low frequency data reduction.

In addition to software limitations, one of the most significant limitations to the original VLSS data reduction was the lack of a sky model at a comparable frequency. In order to calculate the Zernike polynomials for the phase screen to correct the variable ionosphere across the field of view, a sky model was extrapolated from the 1400 MHz NVSS using an assumed standard spectral index of $\alpha = -0.7$. This extrapolated sky model was adequate but led to many false results, where sidelobes of other sources were picked up instead of the real source, which might be much fainter than anticipated; at the same time many steeper spectrum sources which could have been used to improve the solution fits were not included. When considering a re-reduction we quickly realized that we could use the original VLSS catalog itself for a sky model. With no need to estimate source flux, we could focus on true sources in the Zernike fitting, leading to cleaner fits and better solutions.

We have reprocessed all of the VLSS data from the archive to make new maps and a new catalog. The details of the VLSS Redux (VLSSr) maps and

¹Naval Research Laboratory, Code 7213, 4555 Overlook Ave. SW, Washington, DC, 20375, USA.

²National Radio Astronomy Observatory, 520 Edgemont Road, Charlottesville, VA, 22903, USA.

catalogs, will be described in a separate paper. Here we discuss improvements made to the basic data reduction and analysis. In Section 3 of this paper we discuss the data processing including: “smart-windowing” to reduce clean-bias, automated radio frequency interference modeling software, a revised peeling method, and improved ionospheric phase corrections. In Section 4 we present a new “false detection rate” limited cataloging method, and improved ionospheric fluctuation calculations. All of the processing described is implemented in the data reduction package *Obit* [Cotton, 2008], except the ionospheric fluctuations analysis which makes use of additional independent software.

2. The Reprocessing

Here we briefly describe the steps of the reprocessing.

The initial calibration of the data was done in the Astronomical Image Processing Software (AIPS) and remained as described in *Cohen et al.* [2007]. The only change was to eliminate the data-editing steps intended to remove radio frequency interference (RFI); aside from a global clip of very high amplitude data points no editing was done in the initial calibration.

The imaging was a three-step process for each of the 523 pointing centers in the survey. The data were corrected for ionospheric distortions and imaged, and a residual data set with no astronomical signal was produced. Using these residuals the RFI was modeled and that model was removed from the original data set. Corrections for the ionospheric distortions were re-calculated using the RFI-corrected data set and a final field map made. Offset information for the calibrators was kept for use in ionospheric fluctuation analysis.

The pointing center maps were weighted by $1/\text{RMS}$ and combined to create mosaic image squares, in which the overlap of the pointings produces a more uniform sensitivity.

The squares were cataloged by fitting Gaussians to peaks above a given detection level. We cataloged the survey both using the traditional, local 5σ catalog limit, and also using a new method based on predicted false detection rate.

3. Data Reprocessing Improvements

3.1. Field-based Ionospheric Correction

3.1.1. Background

An electromagnetic wavefront passing through the ionosphere will encounter a space and time variable refractive index, which is mainly due to the variable free electron density. A wedge in the integrated electron density (total electron content, or TEC) along the wave’s trajectory will cause a linear phase gradient across an array observing through it, resulting in an apparent position shift for any small source in the field of view. The apparent source position shifts are proportional to the TEC gradient in a given direction and thus may vary across the field of view of the array elements. Higher order phase structures across the array cause a more serious distortion of the wavefront, producing source defocusing, and in extreme cases scintillations [Lonsdale, 2005].

In the regime of linear phase gradients, the “field-based” ionospheric correction method is applicable; it has been described in detail in *Cotton et al.* [2004] and *Cotton* [2005]. The technique is to make a series of snapshot measurements around the locations of known strong sources (calibrators) in the field, deconvolve the images, and estimate the apparent offsets of each. The time sequence of the derived set of source position offsets allows the fitting of a time variable geometric distortion of the sky as seen by the array. Low order Zernike polynomials, which are orthogonal on a circle, are used to model the distortion field. The field is modeled as a phase screen and each position offset measurement gives a 2-D gradient in this screen at the ionospheric puncture point of the line of sight to the calibrator.

At low frequencies with 2-D arrays, some provision must be made for array non-coplanarity [Cornwell and Perley, 1992]. One solution to this problem is the “Fly’s eye” approach where the sky is tiled with many small facets, each tangent to the celestial sphere at its center. In practice, the size of the tile needed is smaller than the isoplanatic patch size (the characteristic scale over which the rms phase difference between two lines of sight is approximately 1 rad, equivalent to a linear size of a few tens of km at 74 MHz [Cotton et al., 2004]) and/or the resolution at which the phase screen can be determined, so a sufficient approximation to de-distorting the sky is to correct each facet for the geometric offset at its center. This is done by calculating the antenna-based phase corrections at the center of the facet and

applying these corrections prior to deriving the dirty image (or residual) of that facet.

An initial Zernike fit is made to each time segment, in which the source offsets are allowed to be arbitrarily large (the limit is set by the user; for the VLSSr 10' was used). This initial distortion model is used to refine the expected source positions. The calibrator offsets are then recomputed using the adjusted model positions. Calibrators are then required to be found within a small radius of the expected position (a sum of 10 pixels plus 10% of the tip-tilt term of the Zernike fit plus the rms of the initial fit). Calibrators with offsets greater than this radius are excluded from further fitting.

An adjustment to the model is made to compensate for possible real differences between the model positions and the data positions (likely for extended sources if the input catalog is not at the same frequency/resolution as the data). The model positions of sources which are flagged in the input catalog as being either resolved or having close neighboring sources are adjusted if the average offset residual for the calibrator over all time intervals exceeds half of the residual RMS for all sources. Calibrators which are both isolated and unresolved in the model are not adjusted.

The fits to the individual time segments are then recomputed and the average residual offset is compared to a target RMS residual, which is essentially the residual "seeing" size that is allowed; in practice we find that a quarter to a third of the synthesized beam is a good choice. If the average RMS of the residuals is greater than the target, the most discrepant remaining calibrator offset which has at least 1.5 times the average variance is rejected and the Zernike fit is recomputed. This is repeated until one of the following conditions is met: 1) the RMS residual is acceptable, 2) there is no calibrator which contributes more than 1.5 times the average variance, or 3) there are too few measurements for a fit. In the latter two cases, this time segment is flagged and excluded from further imaging.

The ionosphere can be extremely variable and at times the data cannot be adequately corrected for its effect with the Zernike fits; these times should be excluded from imaging. They are usually indicated by defocusing; in extreme cases, none of the calibrators can be detected so no field-based calibration is possible. In less extreme cases, the sources are still detectable so they pass the field-based calibration step.

For these data, defocusing can be identified from the peak image values of the calibrators. For each calibrator, the average image peak is determined. If in any time segment, the average ratio of the calibrator peak to its average drops below 50%, the time segment is rejected. 50% was found to be a good compromise in general between removing too much data and keeping poor data when we first started reducing 74 MHz VLA data, but the parameter can be changed in the software if desired. The remaining time sequence of fitted Zernike polynomials is applied in the imaging and deconvolution as was described in *Cohen et al.* [2007].

3.1.2. Improvements for the VLSSr

The field-based calibration used in the processing of the VLSSr differs from the original processing in a number of respects. Principal among these are using the source catalog from the VLSS as the calibrator list and using a higher order Zernike model.

The original VLSS field-based calibration used the NVSS as a sky model. Because this is at a very different frequency and resolution from the data, it was necessary to predict 74 MHz flux values for the sources using an average spectral index of $\alpha = -0.7$. However it was not possible to tell which of the potential calibrator sources would actually be present in the data at that flux. For any calibrator, the true source might not be detectable, and false detections of sidelobes instead of true sources contaminated the calibrator sample used in the Zernike calculations. The high probability of a false detection made it necessary to limit how far from the nominal source position we searched, and thus times with larger ionospheric disturbances were lost. This problem was almost completely eliminated in the VLSSr by using the original VLSS source catalog [*Cohen et al.*, 2007] for the sky model. By using a sky-model at the same frequency and resolution, we are certain that every calibrator source exists at the expected flux in the data, and can therefore include more sources and search for them over a wider shift area without compromising the solutions. There were a few areas on the sky where the original VLSS was incomplete or insufficient for good ionospheric calibration (roughly 2% of the fields); in those cases the NVSS was used.

Because there are a greatly expanded set of reliable calibrators in the sky model, further refinements to the calibrator selection can be made to improve the quality of the Zernike model fits. First, any calibrator measurement in which the integrated value

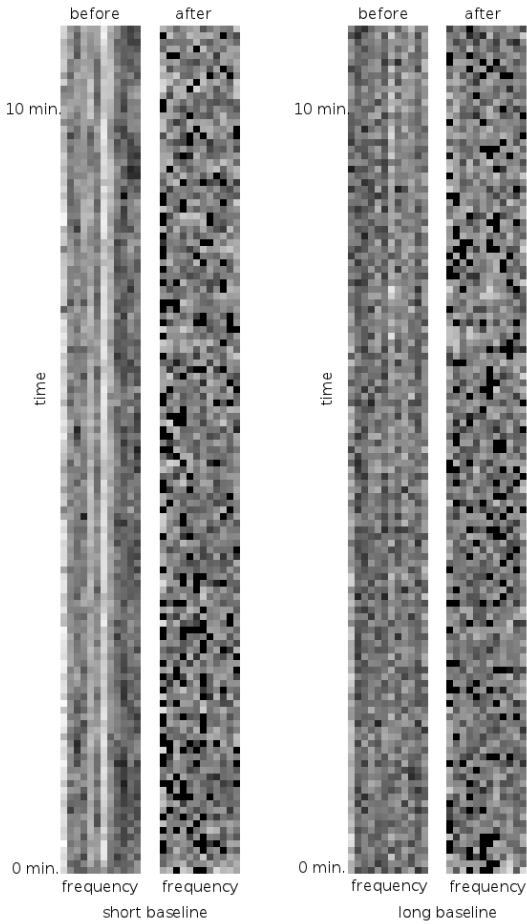


Figure 1.

A short fragment of data on a single baseline is shown before and after applying the RFI removal as described in the text. The baseline on the left is a short baseline (E32-E20) while the data on the right is for a longer baseline (E32-W32). The greyscale is auto-scaled in arbitrary units, with white indicating larger flux values.

is less than a third or more than three times the peak is rejected to remove heavily resolved sources and sidelobes. The next level of filtering is to make a preliminary fit of the Zernike model and restrict the calibrator set to those sources with offsets which do not grossly differ from that model. The Zernike model is then re-fit to the offsets of the final selection of calibrator sources, with all fits weighted by the calibrator peak flux density.

The improved initial sky model and subsequent selection criteria allow the inclusion of more measurements of the ionospheric gradient over a wider

range of spatial scales (see Section 4.2) than in the original reduction.

In the original VLSS we included sources stronger than a predicted flux of 3 Jy (extrapolated from the NVSS), and were, for most fields, forced to model the ionosphere at 2 minute intervals to improve the dynamic range in the offset measurements. The number of sources we could find to model each time interval were few enough that the Zernike solutions were limited to 2nd-order polynomials, and a large fraction of the data was lost when a good solution could not be found during a given time interval.

By contrast, for the VLSSr we were able to reliably use sources with measured total flux of 2.5 Jy or greater and solve for the Zernike polynomials at 1 minute intervals. We ran both 2nd and 3rd order Zernike solutions for all fields. For roughly 70% of the fields, the 3rd order solution produced a “better” map based on the criteria of a higher dynamic range and greater maximum peak flux; we also made sure the two maps had comparable total flux in the field (no sources were lost or power scattered around by one of the two calibration methods). Visual inspection was made of any field where these criteria did not clearly indicate a better map and/or where the total flux values were not comparable.

3.2. RFI Excision

Radio Frequency Interference (RFI) is a persistent problem at lower radio frequencies and can seriously corrupt images. Many of the interfering signals are broadband and/or slowly varying in time making them more difficult to detect than impulsive or narrow band signals. The RFI mitigation strategy used for the VLSSr is a combination of the traditional “flagging” of the most seriously affected data coupled with an RFI estimation and subtraction technique similar to the one described by *Athreya* [2009].

Initial editing of the data removes any visibility measurements with extremely large amplitudes. This allows the data to be imaged and an initial model of the sky to be subtracted from the data. The residual data should be dominated by the RFI and can be used to estimate the effect of RFI on the data; by working on residuals we minimize the chance of removing any real celestial signals during the process.

Stationary terrestrial-based interfering signals should have a constant phase as seen by the array, whereas celestial signals will have a phase which is constantly varying due to the changing geome-

try caused by the rotation of the earth. This earth rotation induced phase variation is removed in the correlation by a process known as "phase tracking". The phase tracking will cause a celestial point source at the phase tracking position to have a constant phase whereas any terrestrial RFI will have a variable phase. This process can be reversed for the residual data, counter-rotating the data by the inverse of the phase tracking. This will cause the terrestrial RFI to have a constant phase and any remaining celestial signals to rotate. Time averaging of this counter-rotated data will further smear out any residual celestial emission but leave constant RFI unaffected.

The averaged counter-rotated residual data can then be filtered to form a time variable model of the RFI. RFI will not be present at all times and baselines so only values above a minimum threshold are accepted in the RFI model. The resulting RFI model then has the phase tracking re-applied. It is interpolated to the data sampling times for each baseline, frequency, and polarization and subtracted from the data. For very short baselines, the difference in the phase rotation of celestial and terrestrial sources may not be sufficiently large to separate them; to compensate, these data are removed completely if they exceed the minimum RFI threshold. The model is subtracted from the original data to produce a data set containing the celestial signals but with the estimate of the RFI removed.

The RFI modeled by the process described above is not always sufficiently constant in time that it can be completely removed by this technique. To compensate for this, the RFI model is also subtracted from the residual data and the times, baselines, frequencies and polarizations of any values with amplitudes above nominal values in I and V are excluded from further processing. Any baseline, channel or IF which has more than 25% of its data excluded by the stokes V test is removed completely. Each baseline is further filtered in the frequency domain by removing frequency channels with an RMS that differs by a chosen amount from the median level during a given time interval. The edited, RFI subtracted data is then ready to be re-imaged.

The RFI estimation process is implemented in Orbit task LowFRFI and is described in more detail in *Cotton* [2009]; the subsequent data clipping is implemented in Orbit task AutoFlag.

For the VLSSr, we found the following parameters gave good results in our early tests. Initial data edit-

ing was done in AIPS to remove all visibilities with amplitudes greater than two times the zero-spacing flux, as estimated by fitting for flux vs. UV-distance and extrapolating back to a distance of zero. For the RFI modeling, the data were averaged for 8 minutes and the minimum RFI amplitude threshold was 0.5 Jy. For the subsequent editing step, data with stokes I flux > 400 Jy or stokes V flux > 300 Jy were removed. For each 10 second sample, frequency channels with an RMS which differed from the median of all channels by more than 6σ were removed.

In the original VLSS we completely removed channels which were part of the 100kHz interference "comb" generated by the VLA itself [*Kassim et al.*, 2007]; however this frequently removed good data as the comb did not appear at equal strengths on all baselines. For the VLSSr we let the RFI modeling algorithm remove the comb. Figure 1 shows VLSSr data on two sample baselines before and after applying the RFI removal steps described here. For the short baseline, although the RFI dominates much of the frequency band, most of the data were able to be retained. Although initially there is far more RFI structure on the short baseline, the RFI-subtracted and flagged data look very similar on both the long and short baselines, without visible interference, and without the necessity of excising large portions of the short baseline.

The original VLSS excluded all baselines shorter than 200λ from the processing to reduce RFI. This limited the theoretical largest angular scale of the survey to $18'$. By using the RFI modeling and removal techniques described here we were able to include all baselines present in the data. This doubles the theoretical largest angular scale in the survey to $\approx 36'$. Because the data do not have complete UV-coverage of any field the actual largest angular scale is lower in both reductions. The increase in extended source sensitivity has a dramatic impact on the appearance of large sources, such as Galactic supernova remnants. Combined with the lower noise values, we also see some new large-scale features in extragalactic sources, such as the radio tails of the galaxies in the center of the cluster A194. Images of two large objects are shown in Figure 2 to illustrate the improvements achieved by the new processing.

3.3. Peeling

Peeling is a term used to mean the calibration, imaging and removal of one source from a data

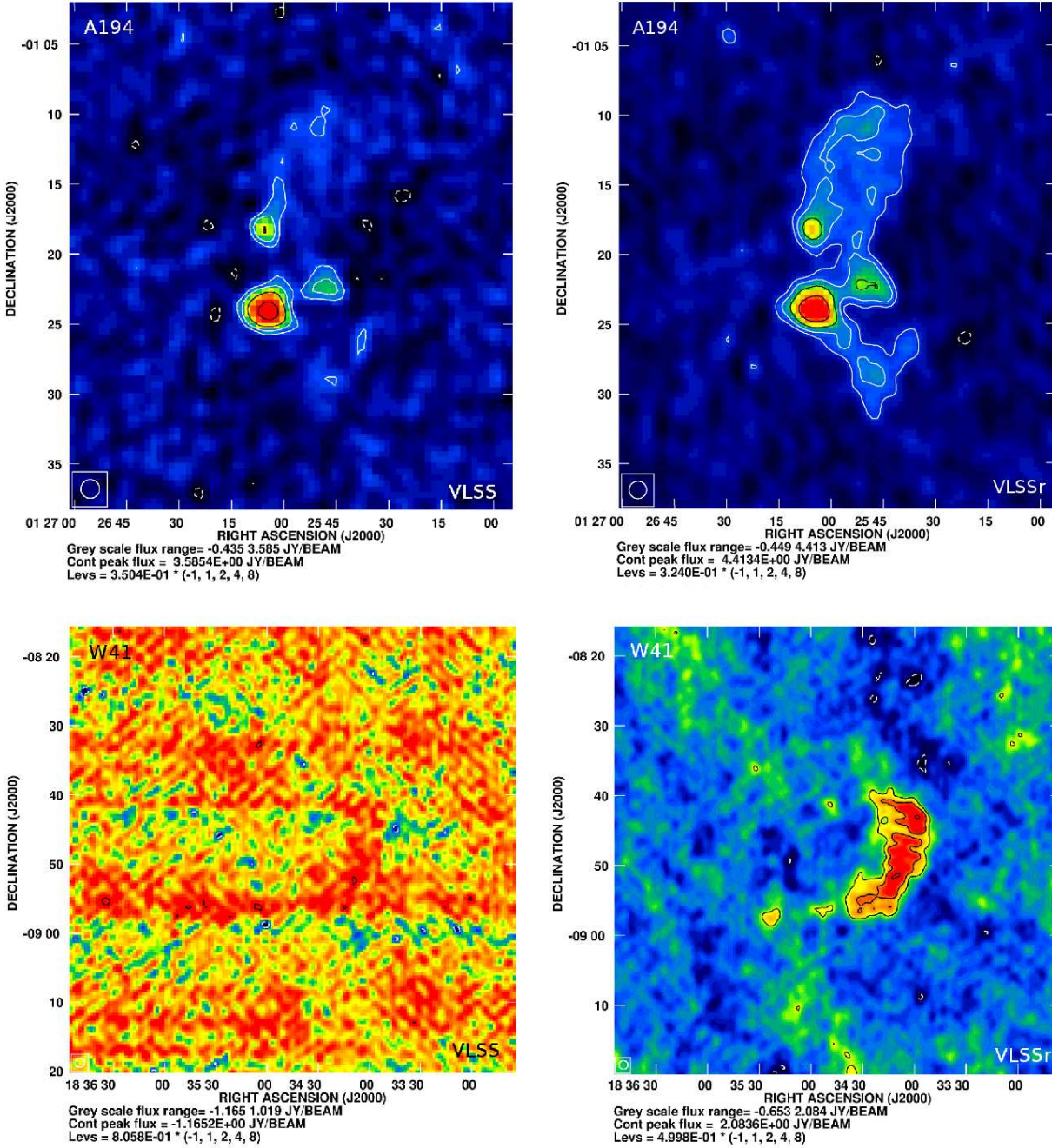


Figure 2. Comparison of the VLSS (*left*) and VLSSr (*right*) for two extended objects. Abell 194 (*top*) is two luminous and distorted radio galaxies at the center of a low-redshift galaxy cluster. The improvement is due to a combination of increased extended source sensitivity and lower noise. W41 (*bottom*) is a giant shell-type supernova remnant in the Milky Way Galaxy. The improvement is due to the improved RFI suppression and the increased extended source sensitivity. Because the VLSS and VLSSr images have slightly different restoring beams and the pixel values are given in Jy/beam, the objects are plotted at equivalent, rather than identical, flux scale ranges based on the minimum and maximum pixel value in each image. Images are contoured at multiples of 3σ .

set, with the goal of better imaging the remaining sources. By removing the source completely, peeling

which can be important for imaging weak sources

in the presence of a very strong source. When many sources are peeled in sequence, it can be used to build up a large scale image where each source has been individually calibrated to remove ionospheric phase terms that are variable across the field of view [In-tema *et al.*, 2009].

Because we had the ability to use field-based calibration to model and correct position-variable ionospheric phase terms, we used peeling only to mitigate the effects of sidelobes from bright sources in the VLSSr. Direction dependent calibration focuses the field of view over which the solutions are valid. If the distribution of calibrators used in the solutions is not optimal so that the phase screen is not calculated over the entire imaging area, or if the ionospheric phase screen is more complicated than can be described by the polynomials, sources may not be ideally focused, and may retain sidelobes. This is particularly true for sources which are not well-centered on a pixel and for sources near the edges of the image. For most sources these are below the RMS noise in the image and can be ignored; however for bright sources they may leave imaging artifacts that we wish to remove by peeling.

The peeling algorithm is included in the Orbit task “IonImage”. A Zernike-based ionospheric phase model is derived using all the data and an initial image is made. If any sources in the image have a peak greater than the chosen limit, they are peeled. All other sources are subtracted from a temporary copy of the dataset and a small image is centered at the bright source position so the source is centered on a pixel. The data undergo several loops of phase self-calibration and re-imaging. For the last loop the data are amplitude and phase self-calibrated before producing a final image and clean-component model. The model is then distorted by the inverse of the calculated self-calibration solutions and subtracted from the original uncalibrated UV-data. The subtracted data are re-imaged and the final peeled source model is reinserted into the map at the end.

The key improvement to this algorithm is distorting the model with the self-calibration solutions rather than the entire data set. Calibrating and then uncalibrating the entire data set to peel a source introduced small errors each time it was done and greatly limited the effectiveness of peeling in the original VLSS survey. As a result, only a few of the very brightest sources on the sky could be peeled. For the VLSSr, we found image improvements with peeling

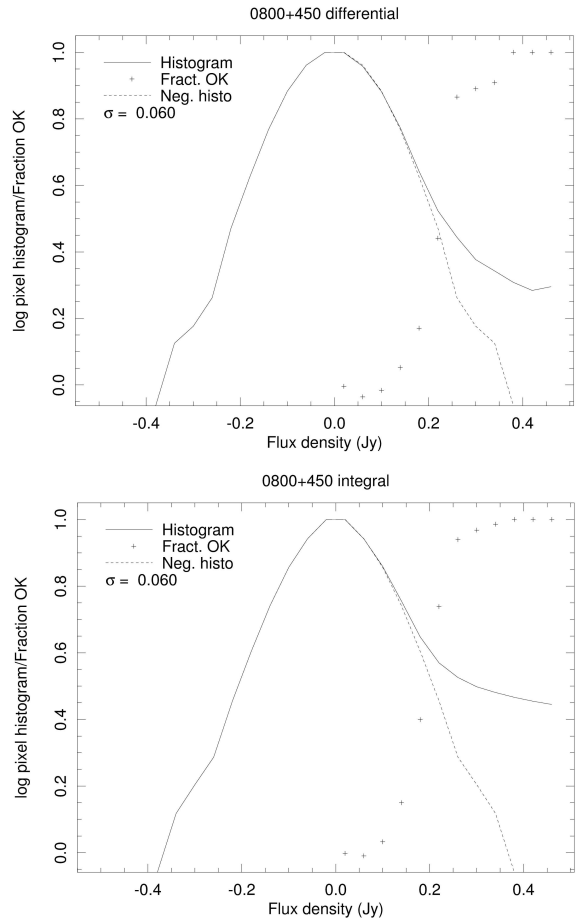


Figure 3. Differential (*top*) and integrated (*bottom*) histograms of the pixel values for a VLSSr square. The solid line shows the histogram. The dotted line shows the negative-pixel value histogram projected onto the positive bins. The plus-signs show the fraction of pixels which represent real sources at a given flux value, assuming the distribution is symmetric.

to much lower levels based on inspection of a subset of fields. All sources with a peak flux > 25 Jy were peeled to reduce sidelobe levels.

3.4. Smart-Window Cleaning

Images deconvolved using the CLEAN algorithm [Högbom, 1974; Schwarz, 1978] are known to suffer from a “clean bias” which systematically reduces the flux of sources in the field (see Condon *et al.* [1998] for a description). This occurs because, as cleaning proceeds to deeper levels, the probability increases that a sidelobe of a source or a noise fluctuation (or

a combination of both) can produce a peak higher than any remaining flux in the image. Cleaning this false source results in flux from its modeled sidelobes being subtracted from the true sources in the field. Therefore, the clean bias results in the flux densities of sources being systematically reduced. The magnitude of the bias is independent of the flux density of sources, but scales with map noise.

One way to reduce the amount of clean bias introduced is to clean only in small areas focused on known real sources. However it can be tedious to set up hundreds of windows around sources in a well-populated low-frequency field; and even harder to know *a priori* how large each window needs to be to include the source but not the surrounding noise.

The Orbit task “Ion Image” includes a “smart-windowing” system which attempts to automatically determine where to clean [Cotton, 2007]. A new box is added to the CLEAN window if the peak residual in a given facet is inside the CLEANable region, but outside the current window, and the peak exceeds five times the residual RMS. The one dimensional structure function of the residual pixel values is then evaluated to determine the size of a round box centered on the peak. The box is given a radius at which the square root of the structure function drops to the greater of 10% of the peak or three times the residual RMS.

While this smart-windowing cannot completely remove clean bias, it does greatly diminish it. Clean bias scales with the local noise, and can therefore be expressed as a multiple of the local noise. As discussed in Cotton [2008], tests using a CLEAN process which is constrained to not clean weak sources deeply show that the windowing can reduce the clean bias to as little as 0.2σ . For the VLSSr using the windowing reduced the clean bias for point sources in our maps by over 50% from 1.39σ in the original published VLSS to 0.66σ in the VLSSr.

4. Improvements to Analysis Techniques

4.1. False Detection Rate Cataloging

Wide-field astronomical images, particularly those intended as sky surveys, are typically decomposed into a catalog of objects. However, pixel values in astronomical images always contain a randomly distributed component, which is unrelated to anything on the celestial sphere. Some criterion must be adopted to distinguish between features in the

image which are a result of this “noise”, and thus unlikely to be real, and sources which do correspond to real objects. The chosen criterion will always involve a trade-off between the possibility of missing real sources and the contamination of the final catalog by false sources.

For cases where the noise has a Gaussian distribution, tests for the statistical probability of any feature being due to the noise distribution are well established. A common, and simple choice, is to make a cutoff at some multiple of the RMS, or σ of the distribution. More sophisticated algorithms for images with Gaussian noise have also been developed [Hopkins *et al.*, 2002; Friedenber *and Genovese*, 2009]. However, low frequency radio images, such as those that form the VLSS, do not have noise with a Gaussian distribution. The poorly known primary antenna pattern and difficulties with modeling the effects of ionospheric fluctuations result in a non-trivial fraction of the celestial power being scattered into fake features. As a result the Gaussian statistics underestimate the number of false detections.

An alternative approach is to estimate the false detection probability directly from the image statistics. If we create a pixel distribution for an image, the negative tail should represent some combination of thermal noise, calibration and imaging artifacts. The positive tail represents those plus real sources. If we assume that the noise should be symmetric, we can estimate the true positive noise from the negative half. The ratio of the excess positive values in a positive flux bin to the negative values in the corresponding negative flux bin equals the fraction of positive values likely to be real sources at that flux value.

$$FDR_x = 1 - \frac{n_+ - n_-}{n_-}$$

where FDR_x is the false detection rate at flux density level x , n_+ is the number of pixels in the positive x bin and n_- is the number of pixels in the negative x bin. In the top panel of Figure 3, a sample histogram of pixel values from one of the VLSSr squares is plotted.

In order to use this method successfully, good statistics well out into the wings of the distribution are needed; this translates to sampling large numbers of pixels. If the character of the noise changes across the map it may be preferred to create statistics over more limited areas. For a survey such as the VLSS, where each map is a mosaic of overlap-

ping pointings, the statistical properties of the noise can be extremely variable.

To make the statistics more robust for smaller numbers of pixels, an integrated pixel distribution can be used; thus each flux bin includes counts of all pixels at that flux or any flux further from zero. The difference in the two distributions can be seen in Figure 3. The calculated false detection rate can then be stated as the probability that a pixel at a given flux or greater is real.

This method allows the person generating the catalog to choose the target false detection rate when making the catalog. When using the resulting catalog, the number of false sources is theoretically known. False detection rate (FDR) cataloging has been implemented in the Obit task FndSou, and can be run on a map subsection of arbitrary size. More details can be found in *Cotton and Peters* [2011].

In order to test the effectiveness of FDR cataloging on the VLSSr we compared the cataloged sources to the much more sensitive NVSS; we would expect only a small fraction of real sources to appear in the VLSS and not the NVSS. Unfortunately, the noise distribution in the VLSSr is not symmetric; there is an excess of positive sidelobes in many areas on the sky. The false detection rate method produced a catalog with 10% more sources than traditional 5σ cataloging tests; however nearly half of those additional sources were fake. When targeting a 1% false detection rate, we achieved closer to a 9% rate, considerably higher than the 5% false detection rate we found using traditional Gaussian (5σ) thresholding. We thus consider the 5σ catalog to be the VLSSr “final” catalog.

4.2. Ionospheric Fluctuation Analysis

The position offset data used within the field-based ionospheric correction of the VLSSr contains a wealth of information about the ionospheric fluctuations present during the observations. *Cohen and Röttgering* [2009] produced a statistical analysis of these fluctuations using the offset data from the original VLSS reduction. Using what are essentially TEC gradient structure functions, they demonstrated that the median behavior of the ionosphere was roughly turbulent, with substantially more activity during the day than at night. The analysis was hampered both by the original VLSS reduction

software and by the ability of the structure functions to characterize individual disturbances.

New software has been recently developed which performs a Fourier-based analysis of the position offset data for all calibrator sources during each observation to produce a three-dimensional (one temporal and two spatial) power spectrum “cube” of TEC gradient fluctuations. These cubes provide a statistical description of the ionospheric environment and allow the identification and characterization of transient phenomena. The technique is described in detail in *Helmboldt and Intema* [2012].

The new software has been applied to the position shifts found in the ionospheric correction step of both the VLSS and the VLSSr; in the latter case information is available both before and after the RFI-mitigation step and both were analyzed. We present a brief overview of the results here; detailed results of this analysis will be presented in a companion paper, *Helmboldt et al.* [submitted]. The top panel in Figure 4 shows the mean two-dimensional power spectrum of fluctuations in the total electron count (TEC) gradient of the ionosphere, while the bottom shows the azimuthally averaged spectra for each of the three data sets. The power spectra are smoothed by the time sampling of 1 to 2 minutes. We have also assumed a single gradient across the array, which smooths the measurements with an 11-km wide kernel (the diameter of the VLA B-configuration). This corresponds to a sinc²-shaped taper of the power spectra which goes to zero at a spatial frequency of $1/11 \text{ km}^{-1}$ or 0.091 km^{-1} . Please see *Helmboldt et al.* [submitted] for more details.

There is a dramatic increase in power on the largest scales (smallest spatial frequencies) between the original reduction, which used the NVSS input catalog, and the current reduction, which uses the VLSS itself for input. As described in Section 3.1.2, this is a reflection of our ability to include sources at larger positional shifts in our ionospheric models, which in turn is a result of having a proper sky model at the data frequency. The larger position shifts correspond to larger-amplitude fluctuations. Note that this also reflects how the improved reduction technique works under more adverse circumstances than previously. Higher average power at low spatial frequencies means on the average a more disturbed ionosphere in the data included.

The accuracy of the the TEC gradient measurement is roughly proportional to the uncertainty of the position offsets which improves with lower noise.

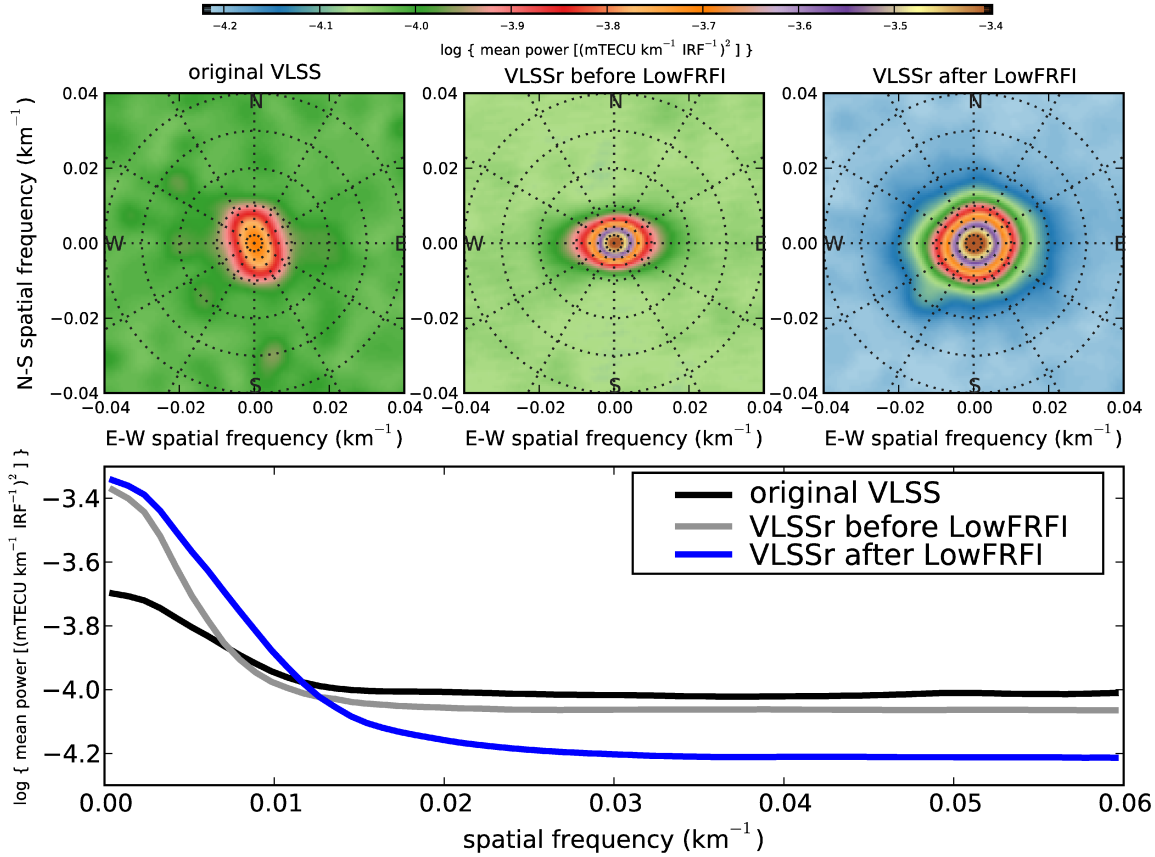


Figure 4. *Top Panel:* Average power spectra of the fluctuations in total electron count (TEC) in two dimensions for the VLSS (*left*), the VLSSr before RFI-mitigation (*middle*) and the final VLSSr (*right*). Data are derived from the calibrator source offsets measured for the field-based calibration. *Bottom Panel:* A radial representation of the power spectrum for the same three data sets. The VLSSr shows an increase in power compared to the VLSS at the smallest spatial frequencies (largest wavelengths). It also has a much lower noise floor allowing the fluctuations to be probed to ionospheric spatial scales that are a factor of 2 larger (corresponding to smaller wavelengths) compared to the VLSS.

So the radial spectrum of the VLSS flattens out due to noise at a spatial frequency of about 0.015 km^{-1} , corresponding to wavelengths less than $\sim 70 \text{ km}$. While the pre-RFI mitigation VLSSr is similarly limited due to noise, there is a dramatic improvement after the RFI mitigation step, which lowered the noise. The post-mitigation spectrum flattens out around spatial frequencies of 0.03 km^{-1} (wavelengths of $\sim 35 \text{ km}$), increasing the range of ionospheric structure scales that can be probed by a factor of two.

5. Conclusions

We have recently reprocessed the VLSS data to create a revised version of the survey, which we call the VLSSr. This new reduction took advantage of improvements to the data reduction process, including an improved peeling algorithm, smart-window cleaning to reduce clean bias, higher order Zernike models to correct ionospheric effects, and RFI modeling techniques. We also investigated a new source cataloging criterion and were able to make an improved and expanded ionospheric analysis based on the ionospheric Zernike model calculations. All of

the improved algorithms except the ionospheric analysis software are available in the Orbit data reduction package.

Although the VLSSr provides a substantial improvement over the VLSS for much of the sky, we were unable to image data from the previously unpublished low declination areas centered near 18 hrs in Right Ascension. These regions were observed twice because the first data were corrupted by extreme ionospheric weather which could not be adequately modeled by the Zernike polynomials. Unfortunately the re-observations were affected by instrumental problems during the recent VLA upgrade, and also cannot be imaged reliably.

Roughly 5% of the remaining fields did not improve with the new reduction techniques. Often these fields exhibit signs of distorted sources just outside the field of view, and/or poor primary calibration. In the original VLSS we self-calibrated many fields to mitigate these types of issues before applying field-based corrections. Because the number of affected fields was so small we chose not to re-introduce the self-calibration step for the VLSSr. The images and source catalogs for these fields are included in the final survey products.

The improved reduction techniques allowed us to image six previously unpublished fields (1%), most near extremely strong sources such as Cassiopeia A. The final catalog includes approximately 95,000 source components, of which 74,000 are unresolved. Sources were fitted with Gaussians which could have maximum sizes of $120''$; larger sources were fitted with multiple Gaussians. In the published VLSS catalog multiple-component sources were summed to create one entry; we have chosen to leave the individual component entries uncombined for the VLSSr.

Comparing the VLSSr to the VLSS, the clean bias was reduced by over 50%, the largest angular scale imaged was approximately doubled, and the number of cataloged sources increased by 35%. We decreased the restoring beam size from $80''$ to $75''$, but average errors on the source positions increased slightly (from $\sim 3''$ to $\sim 3.4''$ in RA and Dec). The new reduction doubles the range of spatial scales over which we are able to measure the power spectrum of ionospheric fluctuations.

Acknowledgments. We would like to thank the referees for helpful questions, comments and suggested revisions. Basic research in radio astronomy at the Naval Research Laboratory is supported by 6.1 base funds. The

National Radio Astronomy Observatory is a facility of the National Science Foundation operated under cooperative agreement by Associated Universities, Inc.

References

- Athreya, R. (2009), A New Approach to Mitigation of Radio Frequency Interference in Interferometric Data, *Astrophys. J.*, *696*, 885–890, doi:10.1088/0004-637X/696/1/885.
- Cohen, A. S., and H. J. A. Röttgering (2009), Probing the Fine-Scale Ionospheric Structure with the Very Large Array Radio Telescope, *Astron. J.*, *138*, 439–447, doi:10.1088/0004-6256/138/2/439.
- Cohen, A. S., W. M. Lane, W. D. Cotton, N. E. Kassim, T. J. W. Lazio, R. A. Perley, J. J. Condon, and W. C. Erickson (2007), The VLA Low-Frequency Sky Survey, *Astron. J.*, *134*, 1245–1262, doi:10.1086/520719.
- Condon, J. J., W. D. Cotton, E. W. Greisen, Q. F. Yin, R. A. Perley, G. B. Taylor, and J. J. Broderick (1998), The NRAO VLA Sky Survey, *Astron. J.*, *115*, 1693–1716, doi:10.1086/300337.
- Cornwell, T. J., and R. A. Perley (1992), Radio-interferometric imaging of very large fields - The problem of non-coplanar arrays, *Astron. Astrophys.*, *261*, 353–364.
- Cotton, W. D. (2005), Lessons from the VLA Long Wavelength Sky Survey (VLSS), in *From Clark Lake to the Long Wavelength Array: Bill Erickson's Radio Science*, *Astronomical Society of the Pacific Conference Series*, vol. 345, edited by N. Kassim, M. Perez, W. Junor, & P. Henning, pp. 337–+.
- Cotton, W. D. (2007), Automatic CLEAN Windowing, *EVLA Memo Series*, (116).
- Cotton, W. D. (2008), Orbit: A Development Environment for Astronomical Algorithms, *Publ. A. S. P.*, *120*, 439–448.
- Cotton, W. D. (2009), Removal of Interference from Low Frequency VLA data, *Orbit Development Memo Series*, *16*.
- Cotton, W. D., and W. Peters (2011), False Detection Rate of Source Finding, *Orbit Development Memo Series*, *25*, 1–4.
- Cotton, W. D., J. J. Condon, R. A. Perley, N. Kassim, J. Lazio, A. Cohen, W. Lane, and W. C. Erickson (2004), Beyond the isoplanatic patch in the VLA Low-frequency Sky Survey, in *Society of Photo-Optical Instrumentation Engineers (SPIE) Conference Series*, vol. 5489, edited by J. M. Oschmann Jr., pp. 180–189, doi:10.1117/12.551298.
- Friedenberg, D. A., and C. R. Genovese (2009), Straight to the Source: Detecting Aggregate Objects in Astronomical Images with Proper Error Control, *ArXiv e-prints*.
- Helmholtz, J. F., and H. T. Intema (2012), Very Large Array Observations of Disturbed Ion Flow from the Plasmasphere to the Nighttime Ionosphere, *Radio Science*, *accepted*, doi:10.1029/2012RS004979.
- Helmholtz, J. F., W. M. Lane, and W. D. Cotton (submitted), Climatology of mid-latitude ionospheric disturbances from the Very Large Array Low-frequency Sky Survey, *Radio Science*.

- Högbom, J. A. (1974), Aperture Synthesis with a Non-Regular Distribution of Interferometer Baselines, *Astron. Astrophys. (Suppl.)*, 15, 417.
- Hopkins, A. M., C. J. Miller, A. J. Connolly, C. Genovese, R. C. Nichol, and L. Wasserman (2002), A New Source Detection Algorithm Using the False-Discovery Rate, *Astron. J.*, 123, 1086–1094, doi:10.1086/338316.
- Intema, H. T., S. van der Tol, W. D. Cotton, A. S. Cohen, I. M. van Bemmell, and H. J. A. Röttgering (2009), Ionospheric calibration of low frequency radio interferometric observations using the peeling scheme. I. Method description and first results, *Astron. Astrophys.*, 501, 1185–1205, doi:10.1051/0004-6361/200811094.
- Kassim, N. E., et al. (2007), The 74 MHz System on the Very Large Array, *Astrophys. J. (Supp.)*, 172, 686–719, doi:10.1086/519022.
- Lonsdale, C. J. (2005), Configuration Considerations for Low Frequency Arrays, in *From Clark Lake to the Long Wavelength Array: Bill Erickson's Radio Science*, *Astronomical Society of the Pacific Conference Series*, vol. 345, edited by N. Kassim, M. Perez, W. Junor, & P. Henning, p. 399.
- Schwarz, U. J. (1978), Mathematical-statistical Description of the Iterative Beam Removing Technique (Method CLEAN), *Astron. Astrophys.*, 65, 345.
- W. M. Lane, Naval Research Laboratory, Remote Sensing Division, Code 7213, 4555 Overlook Ave. SW, Washington, DC 23185, USA. (wendy.peters@nrl.navy.mil)
- W. D. Cotton, National Radio Astronomy Observatory, 520 Edgemont Road, Charlottesville, VA, 22903, USA.
- J. F. Helmboldt, Naval Research Laboratory, Remote Sensing Division, Code 7213, 4555 Overlook Ave. SW, Washington, DC 23185, USA.
- N. E. Kassim, Naval Research Laboratory, Remote Sensing Division, Code 7213, 4555 Overlook Ave. SW, Washington, DC 23185, USA.
- (Received _____.)